ORIGINAL PAPER

physica status solidi a

www.pss-a.com

Check for updates

Investigation of Thermal Stability Effects of Thick Hydrogenated Amorphous Silicon Precursor Layers for Liquid-Phase Crystallized Silicon

Hassan Ali Bosan, Wolfhard Beyer, Uwe Breuer, Friedhelm Finger, Nelli Hambach, Maurice Nuys, Frank Pennartz, Daniel Amkreutz, and Stefan Haas*

The thermal stability of thick (≈4 μm) plasma-grown hydrogenated amorphous silicon (a-Si:H) layers on glass upon application of a rather rapid annealing step is investigated. Such films are of interest as precursor layers for laser liquid-phase crystallized silicon solar cells. However, at least half-day annealing at $T \approx 550\,°C$ is considered to be necessary so far to reduce the hydrogen (H) content and thus avoid blistering and peeling during the crystallization process due to H. By varying the deposition conditions of a-Si:H, layers of rather different thermal stability are fabricated. Changes in the surface morphology of these a-Si:H layers are investigated using scanning electron microscopy and profilometry measurements. Hydrogen effusion, secondary-ion mass spectrometry (SIMS) depth profiling, and Raman spectroscopy measurements are also carried out. In summary, amorphous silicon precursor layers are fabricated that can be heated within 30 min to a temperature of 550 °C without peeling and major surface morphological changes. Successful laser liquid-phase crystallization of such material is demonstrated. The physical nature of a-Si:H material stability/instability upon application of rapid heating is studied.

1. Introduction

Laser-induced liquid-phase crystallization (LPC) technology has been successful in converting amorphous silicon into polycrystalline material of high electronic quality[1–4] and has the potential for low-energy fabrication of crystalline silicon thin-film solar cells on glass.[3,5,6] In the past, several deposition techniques were used to fabricate amorphous or nanocrystalline silicon precursor layers for laser crystallization, the latter involving both solid-phase crystallization below the silicon melting point[5,6] and LPC.[1–4] Major work was done in optimizing absorber layers deposited by electron beam physical vapor deposition (EBPVD) and plasma-enhanced chemical vapor deposition (PECVD).[5–8] By default, PECVD was initially preferred due to its industrial relevance and easy integration into large-scale manufacturing[5] while EBPVD was considered not economically favorable due to the need for expensive silicon ingots for absorber deposition. However, for the PECVD-deposited hydrogenated amorphous silicon (a-Si:H) layers, at least half-day oven annealing at 550 °C had to be used to effectively drive out the H for film thickness ≤5 μm.[9] For thicker a-Si:H precursor films, even longer dehydrogenation procedures were necessary.[9] Without this H removal, the material delaminated during liquid phase crystallization.[9,10] Unfortunately, the slow annealing process increased the manufacturing time and cost. On the other hand, EBPVD-deposited amorphous or nanocrystalline silicon layers did not require a pre-annealing step and offered a superior deposition rate. Hence, EBPVD precursor layers were extensively researched for LPC solar cells and recently, a conversion efficiency of 15.1% for back-contacted 14 μm-thick silicon on glass was demonstrated.[11]

In the present work, we examine the thermal stability of thick PECVD-deposited a-Si:H layers on glass (coated by SiO_x, $SiO_x/SiN_y/SiO_x$ or $SiO_x/SiN_y/Si(O,N)_x$ (ONO type layers)[8,9]) under rapid annealing up to 550 °C. By variation of the PECVD plasma parameters, a-Si:H material was realized that could be dehydrogenated by this rapid annealing process while other films peeled. Details of the peeling process were studied. The enhanced thermal stability of a-Si:H films upon rapid dehydrogenation is associated with a porous structure. With regard to film thickness, we

H. A. Bosan, Dr. W. Beyer, Dr. F. Finger, Dr. N. Hambach, Dr. M. Nuys, F. Pennartz, Dr. S. Haas
IEK5-Photovoltaik
Forschungszentrum Jülich GmbH
Leo-Brandt-Straße, Jülich 52425, Germany
E-mail: h.ali@fz-juelich.de

Dr. U. Breuer
ZEA3-Analytik
Forschungszentrum Jülich GmbH
Leo-Brandt-Straße, Jülich 52425, Germany

Dr. D. Amkreutz
Institut für Silizium Photovoltaik
Helmholtz-Zentrum Berlin für Materialien und Energie GmbH
Kekuléstraße 5, Berlin 12489, Germany

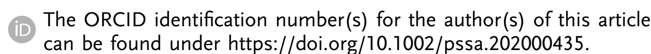
The ORCID identification number(s) for the author(s) of this article can be found under https://doi.org/10.1002/pssa.202000435.

© 2021 The Authors. physica status solidi (a) applications and materials science published by Wiley-VCH GmbH. This is an open access article under the terms of the Creative Commons Attribution License, which permits use, distribution and reproduction in any medium, provided the original work is properly cited.

DOI: 10.1002/pssa.202000435

confine to films of about 4 µm, well aware that recent high efficiencies reached for this type of solar cell involved much thicker films (10–14 µm).[4,9,11] We note, however, that this type of solar cell can be fabricated with efficient light traps requiring rather thin silicon layer thickness. For example, by Green et al. a silicon thickness of 1.4 µm was reported.[5] The final film thickness in a production process will likely depend on the overall economy. Our intention is not to present the recipe for a new type of c-Si thin-film solar cell on glass but to point out that the PECVD technique may supply suitable precursor layers besides EBPVD without a very long dehydrogenation time.

2. Experimental Section

As a substrate for the a-Si:H films, we used Corning Eagle XG (borosilicate) glass covered either with ONO-type interfacial layers[8,9,12] or with an SiO_x layer. Such interfacial layer stacks between the glass and the amorphous silicon precursor layer are intended to fulfill several mechanical, optical, and electronic functions.[9] This includes the function of wetting during the LPC process and acting as a diffusion barrier for impurities from the glass substrate.[9] Another important purpose is the improvement of the sticking of the silicon film to the substrate.[9] The SiO_x layer also serves to improve the sticking of the silicon film to the substrate by avoiding bubble and pinhole formation.[13] Note that much work has been done for the development of such interfacial layers.[8,9,12,14,15] Our ONO interlayers were deposited by PECVD at Helmholtz-Zentrum Berlin (HZB). The typical layer thicknesses were 200 nm SiO_x, 80 nm SiN_y, and 20 nm SiO_x or $Si(O,N)_x$, with the layers deposited in this sequence. Details of this layer stack are discussed in the article by Preissler et al.[12] It was pointed out that well-suited ONO for LPC involves a nearly stoichiometric silicon nitride deposited by PECVD at a rather high (≈400 °C) substrate temperature.[12] We note that previous work showed a low void-related microstructure for this type of PECVD SiN_x:H.[16] The SiO_x layers were deposited at Forschungszentrum Jülich in the 13.56 MHz PECVD cluster tool named JANA. Gas flows of CO_2 and SiH_4 were used. Thick hydrogenated amorphous silicon films (thickness ≈4–5 µm) were deposited onto the ONO (or SiO_x) interlayers inside the JANA PECVD chamber. The a-Si:H layers were prepared at various sets of SiH_4 and H_2 gas flows. Radio frequency (RF) power from 20 W to 90 W and total gas pressure from 1 mbar to 6 mbar were applied. The substrate temperature for both SiO_x and a-Si:H films was kept at $T \approx 300$ °C. To study the thermal stability of the films, the samples of 2×2 cm^2 were heated on a hotplate from room temperature to 550 °C within 30 min. In **Figure 1**, the heating characteristics of our hotplate heating is shown. Heating rates of about 30 °C min^{-1} were applied with intermediate 5 min annealing at the temperatures of 250, 350, and 450 °C.

The changes in the surface morphology and film thickness of a-Si:H layers, after annealing the samples at 250, 350, 450, and 550 °C for 5 min, were investigated using an FEI Magellan 400 scanning electron microscope (SEM) and Veeco Dektak 150 profilometer, respectively. All annealing experiments were conducted in ambient or nitrogen atmosphere. Furthermore, the relative change in the H signal at these annealing steps was measured by Raman spectroscopy using Horiba-Yvon

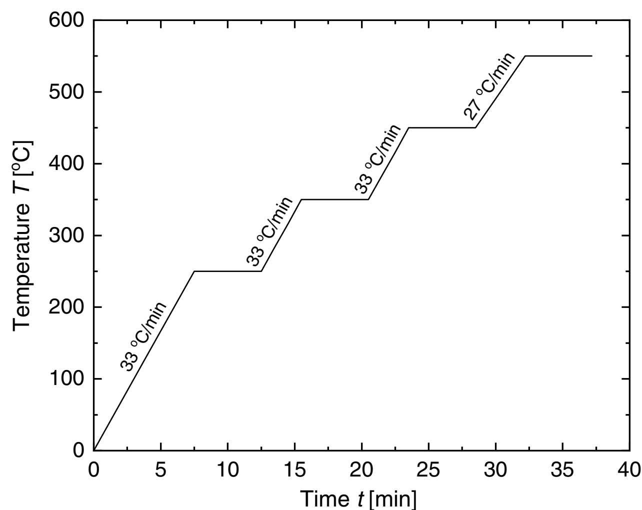

Figure 1. Temperature versus time dependence for the applied hotplate heating.

LabRAM at an excitation wavelength of 532 nm. Raman spectroscopy was also used to measure the H microstructure parameter (R_H)[17], the short-range order (SRO), and the medium-range order (MRO).[18] H concentration (C_H) was measured by Fourier transform infrared spectroscopy (FTIR) on reference a-Si:H samples deposited on crystalline silicon wafer substrates and used for estimating the H concentration in the investigated samples deposited on glass substrates. For both Raman and infrared spectroscopy, the relative H content in the Si–H stretching modes was measured by fitting two Gaussian peaks centered at 2000 and 2090 cm^{-1} to the complex Si–H stretching vibration signal.[17] Hydrogen effusion measurements were performed as reported in the literature,[19] using a heating rate of 20 °C min^{-1}. For secondary-ion mass spectrometry (SIMS) measurements, a time of flight instrument (TOF.SIMS-5.NCS, Iontof GmbH, Münster, Germany) was used. An area of 300×300 µm^2 was sputtered using a Cs ion beam and an area of $\approx 40 \times 40$ µm^2 was measured using a Bi ion beam. The primary purpose of SIMS measurements was to obtain hydrogen depth profiles prior to and after annealing. For structuring, a 355 nm Rofin-Sinar nanosecond laser was used to ablate laser lines into the a-Si:H material to act as artificial vents for H effusion and stress release. The surface of the layers with laser grooves was imaged by a Nikon Eclipse L200D microscope. An 808 nm diode line laser by LIMO GmbH was used for the LPC process. Note that much work has been done for understanding and the improvement of the laser LPC of amorphous silicon.[1–3,7,20]

2.1. Hydrogen Diffusion and Release Processes in a-Si:H

The release of H upon annealing from a hydrogenated material is governed by the H diffusion coefficient D, giving rise to a hydrogen diffusion length L,

$$L = 2(Dt)^{\frac{1}{2}} \tag{1}$$

where t is the annealing time. For the depletion of H from a-Si:H films to avoid blistering and bubbling effects[10] during LPC, the

© 2021 The Authors. physica status solidi (a) applications and materials science published by Wiley-VCH GmbH

H diffusion length needs to be at least equal or needs to exceed the film thickness. On the other hand, during the H depletion process, the solid-phase crystallization of a-Si:H should be avoided, as this process often leads to material rupture and delamination.[21,22] Blum and Feldman[23] have published a formula describing the solid-phase crystallization process of a-Si:H by the temperature dependence of the crystallization (incubation) time t_c. According to this formula ($t_c = 5 \times 10^{-14}$ s exp (3.1 eV/kT)), crystallization will take place after more than 100 h of annealing at 550 °C for undoped a-Si:H. To estimate the H diffusion length according to Equation (1), the H diffusion coefficient in a-Si:H at the annealing temperature T is required. It is known, however, that depending on H concentration, material density, and microstructure, H can diffuse in a-Si:H by both atomic H and H_2 molecules.[13,24,25]

For device-grade ("dense") a-Si:H, H diffusion has been shown to proceed by the motion of H atoms.[24] For the Arrhenius parameters of this latter H diffusion process, it was found that they depend on various variables, in particular on H concentration.[26] Thus, without detailed material analysis, only estimations on the H diffusion length for a given annealing temperature and annealing time are possible. Using literature data for the Arrhenius dependence $D = D_0$ exp $(-E_D/kT)$ of H diffusion in dense a-Si:H (with a hydrogen concentration of about 14 at.%) by Carlson and Magee[27] ($E_D = 1.53$ eV, $D_0 = 1.17 \times 10^{-2}$ cm^2 s^{-1}) and by Beyer and Wagner[28] ($E_D = 1.49$ eV, $D_0 = 1.1 \times 10^{-2}$ cm^2 s^{-1}), and assuming that for H depletion of a 4 μm-thick film at least a hydrogen diffusion length of ≈10 μm is required, one obtains annealing times at 550 °C of 15 and 9 h, respectively, i.e., of the order of magnitude proposed by Gabriel et al.[9] Note that the influence of the film thickness on H release from dense a-Si:H is directly seen in H effusion measurements which show considerably higher temperatures of the maximum H effusion rate with increasing film thickness.[29,30] Using the formulae and data for H diffusion of dense a-Si:H from literature,[28] for a film thickness of 4 μm the H effusion peak temperature is estimated to be at $T \approx 730$ °C.

From H effusion data it is also known that hydrogenated amorphous silicon films can be prepared which show the major H effusion (heating rate: 20 °C min^{-1}) near a temperature of 500 °C[13,25] almost independent of film thickness. This behavior is attributed to the presence of a less-dense a-Si:H material or a-Si:H material with a void-related microstructure, so that in these films hydrogen (H_2) molecules can diffuse with a considerably higher diffusion coefficient than generally found for diffusion by H atoms. In literature, such H_2 effusion behavior has been often observed upon argon (Ar) dilution of silane during deposition, giving rise to columnar a-Si:H growth.[13,31] For such material, the H diffusion coefficient versus temperature has been measured by Street and Tsai.[32] However, since Ar may get incorporated into such films and may cause problems during LPC, we decided rather to search for deposition conditions giving rise to a void-related microstructure and an effusion peak at $T \approx 500$ °C without Ar dilution. As a direct way to identify suitable deposition parameters, we deposited films of about 4 μm thickness and subjected them to the heating procedure shown in Figure 1, searching for stable material.

3. Results

3.1. Material Development

Searching for annealing-stable a-Si:H material, films of about 4 μm thickness were deposited using various flows of silane (SiH_4) and hydrogen. RF power (13.56 MHz) between 20 and 90 W was applied and the total gas pressure ranged from 1 to 6 mbar. A stable material was obtained in a quite limited parameter range, as shown in **Figure 2**. This figure shows an overview of the stable and unstable (peeling) material for a fixed RF power of 20–25 W (diameter of circular electrode: 160 mm) and a total gas pressure of 1 mbar. Only material deposited with a silane flow of 6 sccm and a hydrogen flow of 12 sccm remained stable after our rapid heating procedure. We obtained such stable material on both SiO_x and ONO interface layers. A higher RF power than 25 W resulted in peeling. We also got stable material for the latter silane and hydrogen flows and an RF power of 25 W for total gas pressures of 0.5 and 2 mbar.

In **Figure 3**, the hydrogen effusion rate (heating rate: 20 °C min^{-1}) for such a film of 3.7 μm thickness (using an SiO_x interface layer) is shown as a function of temperature. The deposition rate of this film was about 3 Å s^{-1}. Note that the strongly increasing H background at high temperatures arises from the Corning glass substrate which contains some H. The effusion curve for H with an effusion peak near 500 °C shown in Figure 3 is very similar to the curve reported for Ar-diluted electron cyclotron resonance (ECR) plasma material in literature.[13,25]

3.2. Material Characterization

The distribution of H in the stable a-Si:H material was studied by SIMS depth profiling. In **Figure 4**, the depth profiles of silicon (^{28}Si), oxygen (^{16}O), and hydrogen (^{1}H) are shown for the as-deposited material (Figure 4a) as well as for material annealed

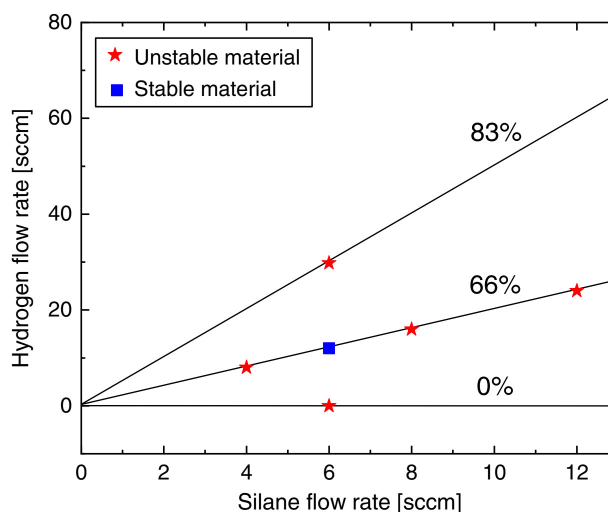

Figure 2. Variation of hydrogen and silane gas flow rates for the preparation of a-Si:H precursor layers. RF power was 20–25 W and total gas pressure was 1 mbar. Lines represent the hydrogen dilution percentages while the red asterisks represent the samples that turned out to be unstable. Thermally stable material is represented by the blue square.

© 2021 The Authors. physica status solidi (a) applications and materials science published by Wiley-VCH GmbH

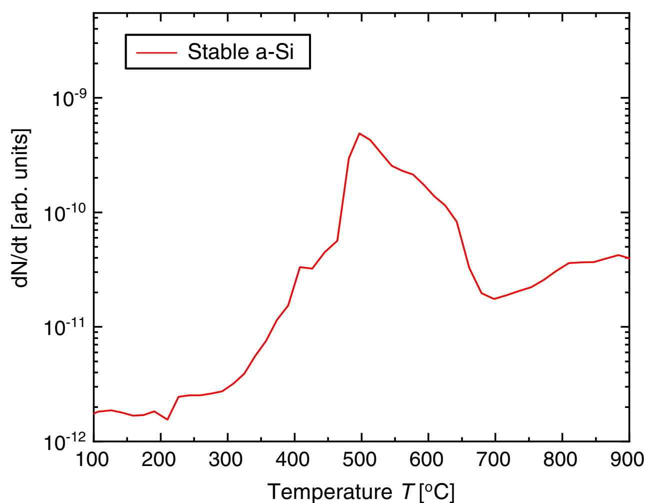

Figure 3. Hydrogen effusion rate dN/dt as a function of temperature T for a stable a-Si:H film of 3.7 μm thickness on SiO_x-coated Corning glass substrate, measured with a heating rate of 20 °C min^{-1}.

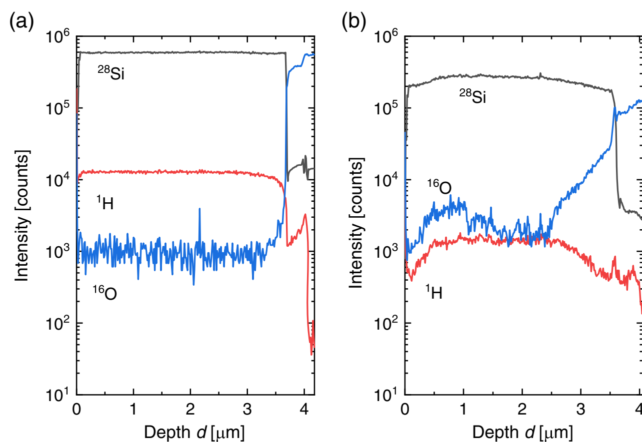

Figure 4. Silicon, hydrogen, and oxygen SIMS depth profiles of thick films of thermally stable a-Si:H, a) as-deposited and b) after annealing (heating schedule see Figure 1) at 550 °C for 5 min.

at 550 °C for 5 min (Figure 4b). The non-constant and, compared with Figure 4a, reduced intensity of the ^{28}Si signal in Figure 4b is presumably due to charging effects in the H-depleted ranges of the material by the Bi ion beam used in the SIMS experiment. Charging is known to distort the ion optics and can reduce the overall SIMS signals greatly.[33] At a higher H concentration in the a-Si:H (as is the case in the as-deposited material), charging is reduced because of the higher photoconductivity of a-Si:H (our SIMS measurements were carried out under illumination) and/or a higher doping effect in a-Si:H of the cesium[34] used for the SIMS sputtering process. A comparison of Figures 4a,b suggests that the "charging effect" arises because the lateral (electrical) conductance of the a-Si:H film decreases by annealing. Concerning the depth dependence of the oxygen signal in Figure 4b, at first sight, one may presume oxygen in-diffusion from the oxide layer. However, no clear in-diffusion of oxygen is visible from the film surface except for some enhancement of the oxygen signal in particular at a depth near 0.5–1 μm from the surface. While in a porous material the diffusion of oxygen-bearing molecules like O_2 or H_2O may be expected through the pores, such migration would primarily be expected from the surface side where these molecules are present but not from the substrate side where basically oxygen is present in bonds to silicon. Thus, we note that the enhanced oxygen signal near the surface may indeed be affected by the annealing process in air, i.e., oxygen in-diffusion. Since oxygen contamination may likely affect the photovoltaic properties of the crystallized material, this result suggests that the dehydrogenation of the porous a-Si:H material should be done under an inert gas or in vacuum. In contrast to the film surface, the O signal near the substrate is likely caused by pinhole formation during the SIMS depth profiling, i.e., by an artifact related to the SIMS measurement.[35] In the latter case, small pinholes (reaching to the substrate) form during the SIMS sputtering process and get larger when the SIMS sputtering crater approaches the a-Si:H/substrate interface.[35] Thus, in the present case, an oxygen signal from the SiO_x layer is detected that gets larger by the SIMS sputtering time, resembling an oxygen diffusion profile. Regarding the H in the material, it is seen that the SIMS H signal (as compared with the silicon signal) is strongly reduced by the annealing procedure to less than one-quarter. Furthermore, it is important to note that in the annealed state (Figure 4b) the H shows an out-diffusion profile, i.e., a decrease in H concentration towards both the film surface and the film–substrate interface.

Both the H effusion peak near 500 °C of Figure 3 and the H out-diffusion profile of Figure 4b (for 5 min annealing at 550 °C) disagree with the published H diffusion coefficients in dense a-Si:H material,[24,27,28] in which H diffusion is known to proceed by the motion of H atoms. The present results rather suggest that H diffusion in our stable material proceeds by motion of H_2 molecules. These molecules cannot diffuse in dense a-Si:H, lacking the space, but apparently can do so in our stable a-Si:H, likely due to reduced material density and/or the presence of microstructure.[13,25] Since the depth profile of H after 550 °C annealing (Figure 4b) suggests H release limited by H diffusion, the H diffusion quantity D/E_D can be determined from the H effusion peak temperature of Figure 3 according to Beyer and Wagner[28] by

$$D/E_D = d^2\beta/\pi^2 k T_M^2 \quad (2)$$

where d is the film thickness, β is the heating rate, k is the Boltzmann constant and T_M is the effusion peak temperature (temperature of maximum effusion rate). Although Equation (2) was originally derived for the out-diffusion of atomic H for a dense material,[28] it can be applied to any out-diffusion process (governed by an Arrhenius dependence) from a thin film proceeding towards both film surface and film–substrate interface. With a film thickness of $d \approx 3.7$ μm and the heating rate of 0.33 K s^{-1} (20 °C min^{-1}), a value $D/E_D \approx 8.9 \times 10^{-11}$ $cm^2\,s^{-1}\,eV^{-1}$ is obtained and is shown as a blue triangle in **Figure 5**. For comparison, data for H diffusion in dense a-Si:H (curve 1) as well as for the material with columnar growth (curve 2) are included. Curve 1 relates to data by Carlson and Magee[27] ($D = 1.17 \times 10^{-2}$ $cm^2\,s^{-1}$ exp $(-1.53\,eV/kT)$), which have been attributed to diffusion by H atoms.[24,27,28] Curve 2 refers to

© 2021 The Authors. physica status solidi (a) applications and materials science published by Wiley-VCH GmbH

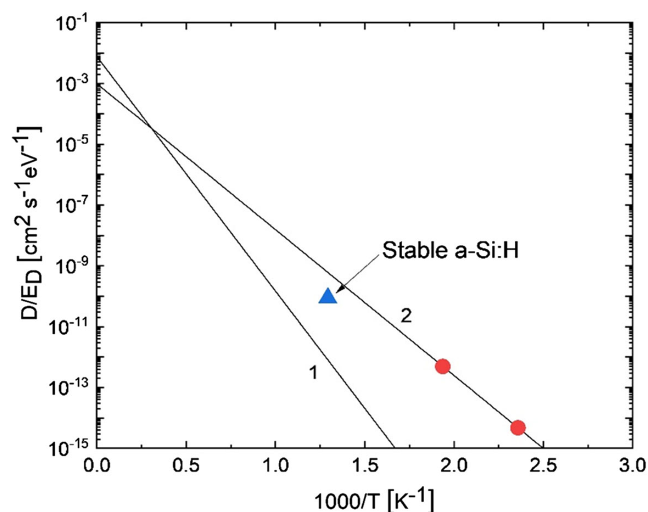

Figure 5. Hydrogen diffusion quantity D/E_D as a function of 1000/T for our stable a-Si:H (blue triangle) as well as literature data for dense a-Si:H by Carlson and Magee[27] (curve 1) and for a-Si:H with a columnar microstructure by Street and Tsai[32] (curve 2, including two data points [red dots]).

data by Street and Tsai.[32] Here, the red dots are experimental values and the line is the fit proposed by these authors ($D \approx 10^{-3}\text{cm}^2\,\text{s}^{-1}$ exp $(-1.0\,\text{eV}/kT)$). The results of Figure 5 show that both our data point and the D/E_D values by Street and Tsai[32] (curve 2) lie at the temperature of 500 °C ($10^3/T \approx 1.3\,\text{K}^{-1}$) and below by two orders of magnitude and more above the atomic H diffusion coefficient (curve 1), supporting that we deal with diffusion by H_2 molecules.

We note that in the case of a-Si:H prepared by Ar dilution, the assignment of a hydrogen effusion peak near 400–500 °C for thick a-Si:H films to diffusion of H_2 is also supported by effusion measurements of implanted neon. It was found that neon which is known to have a similar size as a hydrogen (H_2) molecule[19] effuses at similar temperatures as H for such material.[36,37] For out-diffusion of hydrogen from (porous) a-Si:H with diffusion of H_2, the details of the ONO interface layer (with respect to film peeling) appear much less critical than for dense a-Si:H material, as all H can in principle diffuse out through the film surface, apart from the fact that such films are expected to grow with less internal strain than dense a-Si:H films.

We also studied thick films of a-Si:H deposited at a higher deposition rate than that used for the stable material, as such precursor material could further reduce the fabrication time (and costs) of LPC silicon solar cells. For the deposition conditions with H dilution of 95% (SiH_4 flow 12 sccm, H_2 flow 228 sccm), gas pressure of 6 mbar, and RF power of 90 W (13.56 MHz), we achieved a deposition rate of 12 Å s^{-1}, i.e., a factor of 4 higher than the growth rate of our stable material. To obtain a film thickness of about 4 µm, only a deposition time of about 1 h was necessary.

However, this latter material turned out to peel during the rapid annealing procedure. We term it "unstable material" in this article. The reason for the instability of the film (which was deposited on an ONO-coated glass substrate) is investigated in more detail as it may help to find strategies to deposit stable precursor layers with higher growth rates.

Searching for differences between the two amorphous silicon materials (our stable and unstable materials), we evaluated Raman spectra in terms of H concentration as well as with regard to three microstructure parameters termed SRO, MRO, and the H microstructure parameter R_H. Here, SRO and MRO refer to the structure of the amorphous silicon network while R_H refers to H bonding. The width of the Raman a-Si transverse optical (TO) phonon vibration near 480 cm^{-1} has been shown to be related to the SRO (i.e., the mean deviation $\Delta\Theta_b$ (in degrees) from the tetrahedral angle[38]) by

$$\text{SRO} = \Delta\Theta_b = (\Gamma_{TO} - 15\,\text{cm}^{-1})/6. \quad (3)$$

Here, Γ_{TO} is the linewidth of the TO phonon vibration in units cm^{-1}.

For the characterization of MRO, i.e., the rotational alignment of the silicon tetrahedra to each other, the ratio of the integrated transverse acoustic (TA) and TO Raman modes has been proposed,[18,39,40] i.e.,

$$\text{MRO} = I_{TA}/I_{TO}. \quad (4)$$

In this definition, a higher MRO parameter means higher disorder[18] and for crystalline silicon with all tetrahedra aligned, MRO = 0. Thus, MRO is particularly useful to describe the transition from amorphous to (micro-)crystalline silicon. For the characterization of the MRO of fully amorphous silicon, 1/MRO appears more useful than MRO. According to literature data, device-grade a-Si:H has values near 1/MRO ≈ 4–5.[41] To our knowledge, the highest values reported for a-Si:H without microcrystalline inclusions did not exceed 1/MRO ≈ 5.2.[42,43]

The H microstructure parameter uses the fact that the frequency of the Si–H vibration is different if Si–H vibrates in a dense material or at a surface.[44] In a dense material, Si–H vibrates at a frequency near 2000 cm^{-1} while at a surface, the vibration is near 2090–2100 cm^{-1}.[44,45] Thus, the ratio

$$R_H = I(2100\,\text{cm}^{-1})/(I(2100\,\text{cm}^{-1}) + I(2000\,\text{cm}^{-1})) \quad (5)$$

of vibrational intensities I is a measure of the concentration of surface-bonded H and thus (roughly) of the concentration of voids. The results for these microstructure parameters of our two a-Si:H materials are shown in **Table 1** along with H concentration.

According to Table 1, the hydrogen concentration C_H of the unstable material is considerably higher than that of the stable material (almost 12 at.% and nearly 8 at.%, respectively). We note that the reduced H concentration of the stable material may be

Table 1. Comparison of hydrogen concentration (C_H), short range order (SRO), medium range order (MRO), reciprocal MRO (1/MRO), and hydrogen microstructure parameter (R_H) for thermally unstable and stable a-Si:H materials.

Type	C_H [at.%]	SRO [deg.]	MRO	1/MRO	R_H
Thermally unstable	11.6	8.80	0.193	5.18	0.101
Thermally stable	7.74	8.70	0.234	4.27	0.153

© 2021 The Authors. physica status solidi (a) applications and materials science published by Wiley-VCH GmbH

due to the lower deposition rate but may also be connected to deposition under conditions of H depletion[32] which is considered to cause columnar growth and microstructure. As shown in Table 1, furthermore, there is little difference in SRO between the two materials and the values $\Delta\Theta_b \approx 9°$ are right in the middle of experimental data (7.7°–10.5°) noted by Beeman et al.[38] From this result of a similar SRO for the different materials, one may conclude that either the concentration of interconnected voids is not very high and/or that the void surfaces are not depleted of H in the stable material.

Finally, the H microstructure parameter R_H in Table 1 is found to be lower in the unstable material compared with the stable one. This result agrees with the presence of a higher concentration of H-covered voids in the stable material compared with the unstable material. In summary, we conclude that the measured microstructure parameters agree with the assignment of the unstable material to a dense a-Si:H while our stable material is less dense, having a (void-related) microstructure as clearly detected also by H effusion (see Figure 3).

The SEM images of the stable a-Si:H film shown in **Figure 6**e–h illustrate a relatively unchanged surface roughness at each annealing step. Only small craters appear at the surface for annealing up to 550 °C. This thermally stable a-Si:H material is suitable for the LPC process. This is not the case for the thermally unstable material, as shown in Figure 6a–d. This a-Si:H material shows already in the as-deposited state bubbles and pinholes, similar to that reported by Shanks et al.[46,47] After annealing at 350 °C, the film peeled off over most of the area of the sample, leaving behind only a film of 400–500 nm thickness with lots of pinholes (≤30 μm in diameter) which go down to the film–substrate interface. **Figure 7**, showing the 350 °C-annealed material illuminated with white light from the backside, shows in black a fraction of the original film. The brown area is the 400–500 nm film and the yellowish-white dots are the pinholes going down to the substrate. At higher annealing temperatures, only this 400–500 nm layer remained with basically unchanged pinhole distribution. Because of this peeling effect, this unstable reference material is not usable for LPC.

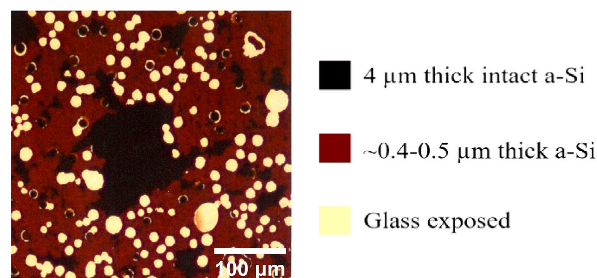

Figure 7. Top-view trans-illumination microscope image of a-Si:H film after annealing (5 min of annealing time) at 350 °C.

We note that pinhole formation in a-Si:H films as visible in Figure 7, has been reported quite often in literature[29,48–51] since first described by Shanks et al.[46,47] It has been attributed to a poor a-Si:H–substrate interface and the build-up of H_2 pressure in cavities at this interface upon H out-diffusion into these cavities from a-Si:H during film deposition and/or upon annealing. According to Figure 6a, such pinholes and bubbles are present in our unstable material already in the as-deposited state. It was pointed out that bubble and pinhole formation is characteristic for substrates with little solubility and diffusion of H_2 (like crystalline silicon or sapphire) while for fused silica or molybdenum substrates it is less or not observed.[13,47]

Due to the higher deposition rate of our unstable a-Si:H material compared with our stable material, the nature of the peeling effects is of interest. We studied the peeling effects of such material by SIMS depth profiling, searching in particular for the reason of peeling at a distance of 400–500 nm from the substrate which was characteristic for unstable a-Si:H deposited under various deposition conditions. **Figure 8** shows the profiles of silicon (^{28}Si), hydrogen (^{1}H), oxygen (^{16}O), and nitrogen (^{42}SiN) as a

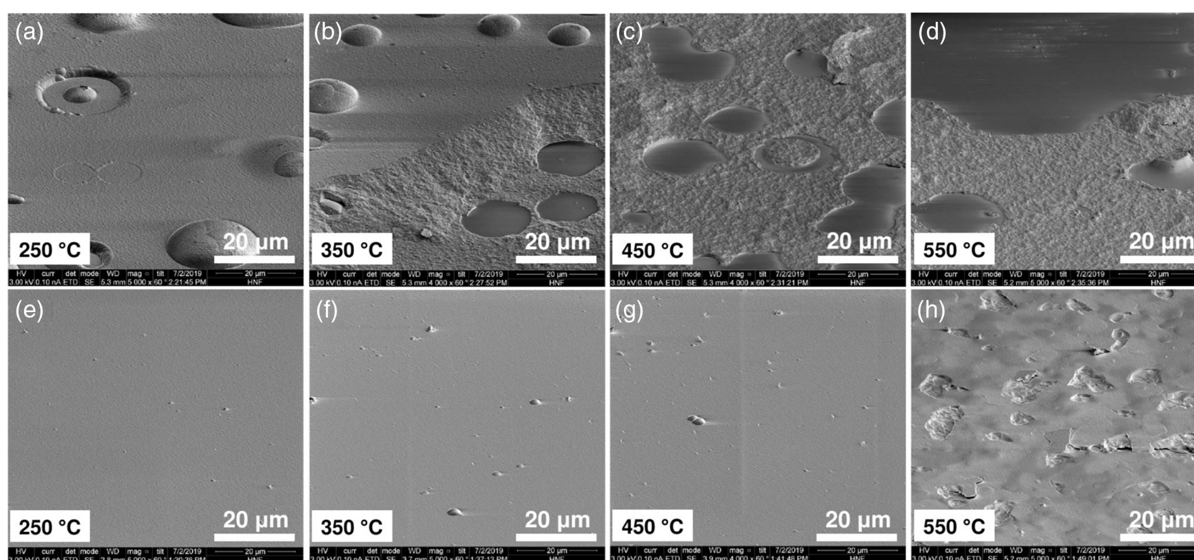

Figure 6. SEM images of a-Si-H surface for both a–d) thermally unstable and e–h) thermally stable a-Si:H films annealed at 250, 350, 450, and 550 °C. For heating schedule and annealing time (5 min), see Figure 1. Each image is tilted 60° to the surface plane. Space bar (20 μm) is indicated.

© 2021 The Authors. physica status solidi (a) applications and materials science published by Wiley-VCH GmbH

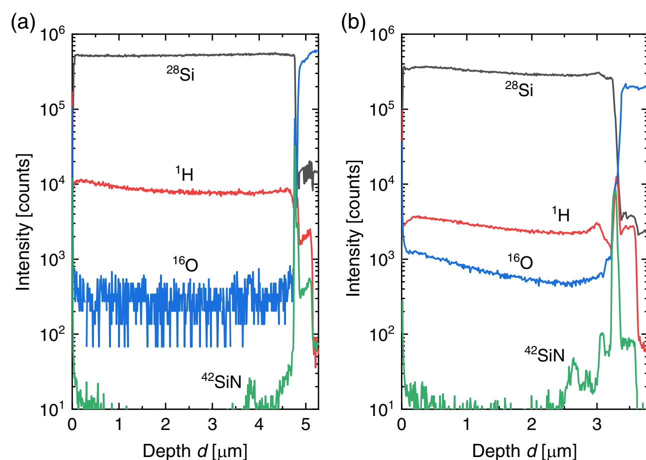

Figure 8. SIMS depth profiles of silicon, hydrogen, oxygen, and nitrogen (SiN) for our unstable a-Si:H, a) as-deposited and b) after annealing at 350 °C for 5 min.

function of depth. The profiles of the as-deposited material are shown in Figure 8a. Enhanced signals of O and SiN reflect the details of the interface which is made up of an ONO layer on top of borosilicate glass. The H signal of the as-deposited material is fairly smooth throughout the film depth, increasing somewhat towards the surface of the film. Such dependence may be caused by H out-diffusion during film growth. However, as the film was deposited near $T_S = 300\,°C$, we expect little H out-diffusion during deposition, as the H diffusion coefficient of dense a-Si:H[27] at 300 °C gives for a deposition time of 1 h only $L \approx 0.02$ μm. We rather think that probably (by unknown reasons) during the deposition process the deposition rate increased slightly which is known to enhance H concentration. Figure 8b shows the depth profiles of the film for the annealing temperature of 350 °C measured close to the edge of the sample where the full film was still present. The film thickness at this sample edge is somewhat reduced.

As it is seen in Figure 8b, the H signal (in relation to the ^{28}Si signal) is slightly lower and the oxygen signal is slightly higher compared to Figure 8a, presumably due to the lower deposition rate at the sample edge, but interestingly the H signal shows some maximum at about 400 nm from the a-Si/ONO interface. Apparently, this H maximum marks the plane where most part of the film peeled off. As an explanation for the peeling at this particular depth of 400–500 nm, we propose void generation caused by inhomogeneous material shrinking[52] paired with stress and the filling of these voids or bubbles by H_2 during annealing. The stress likely arises next to the substrate by the different thermal expansion coefficients of a-Si:H and the glass substrate. Then, a scenario similar to "smart cut" in c-Si appears conceivable.[53] While (apart from pinhole formation) the a-Si:H film sticks fairly tight to the glass-ONO substrate, it may peel at a plane defined by stress-related (microscopic to macroscopic) void formation and the filling of such cavities by molecular H_2 at enhanced pressure. This molecular H_2 originates apparently from the diffusion of atomic H in the dense a-Si:H material to the cavity surfaces and the desorption of H_2 from the void/cavity surface into the cavity. This latter process of surface desorption is known

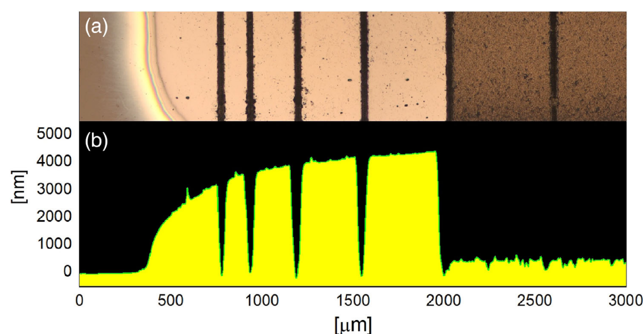

Figure 9. a) Top-view microscope image and b) side-view profilometer thickness profile of the a-Si:H surface of the unstable a-Si:H film with laser ablation lines, after annealing up to 550 °C (5 min annealing time).

to proceed with a free energy of about 2 eV and is expected to give at about 350 °C significant H effusion rates.[19]

To further study the peeling of material for the thermally unstable a-Si:H due to strain and H accumulation (under enhanced pressure) in voids and cavities, laser lines were ablated. A laser beam width of 35 μm and an average power of 190 mW was utilized using a 355 nm nanosecond laser. The a-Si:H material was ablated in a line until the glass substrate was exposed. The distance between the laser-ablated lines was varied from 100 to 1000 μm in 100 μm steps. These lines are intended to act as a strain relief and artificial vents for the effusion of molecular H, accumulating during heating in voids or bubbles in the substrate-near range of the film. The material with these laser lines was then heated in the standard way within 30 min to 550 °C. In **Figure 9**, the top-view microscope image and the profilometer thickness profile of this sample are shown. As demonstrated, the a-Si film survived for a line (vent) distance of 400 μm or less. At a vent distance of 500 μm or more, a-Si material peels off and the film thickness is strongly reduced. These results support that indeed the strain paired with a lack of vents (or of interconnected voids) leads to peeling of the dense a-Si:H material.

The decrease in H concentration at each annealing step of our two materials was also monitored by Raman measurements in the range of the Si–H stretching vibrations, as shown in **Figure 10**a,b. Note, however, that the information depth of Raman depends on the absorption of Raman laser light in a-Si:H and is here in the order of 30–50 nm.[17] For thermally stable a-Si:H material (see Figure 10b), the H signal decreases rather gradually as expected for H out-diffusion and agrees with the SIMS H out-diffusion profile of Figure 4b. For the thermally unstable material (see Figure 10a), on the other hand, we observe a sharp decrease in H signal near $T \approx 350\,°C$. As shown earlier (see Figure 7), we also detected the material peeling at this temperature of 350 °C. Thus, we attribute the strong decrease of the H signal for annealing near 350 °C to the peeling of the major part of the film so that only material next to the substrate remains. We note that the H out-diffusion towards the substrate, as shown in Figure 8b by a small decrease in H concentration next to the ONO interface, involves likely H_2 diffusion in a lateral direction[28] near the a-Si:H/ONO interface where also bubble and pinhole formation takes place already during film growth.

© 2021 The Authors. physica status solidi (a) applications and materials science published by Wiley-VCH GmbH

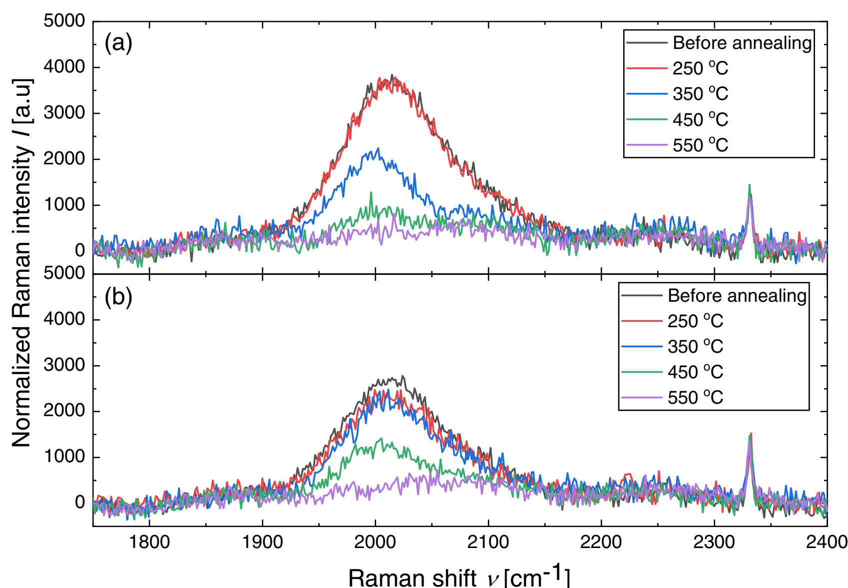

Figure 10. Relative change in the Raman hydrogen signal at different annealing temperatures. For annealing schedule and annealing time (5 min), see Figure 1. The Raman peak centered near 2000 cm^{-1} decreases with increasing annealing temperature. The decrease in the peak intensity is rather sharp at an annealing temperature of 350 °C for the a) thermally unstable material in comparison with smoother decrease for the b) thermally stable material.

3.3. LPC of Stable a-Si:H Dehydrogenated by Hotplate Annealing

LPC was conducted on the stable a-Si:H material deposited on ONO-coated Corning glass which had been heated to 550 °C within 30 min prior to the LPC process. For the laser crystallization process, an 808 nm diode (continuous wave) laser with a beam length of 1.24 cm and a (Gaussian) beam width of 60 μm was used. Various (average) laser powers and scan speeds were applied. At low average laser power, a-Si was crystallized to small grains of micrometer dimensions, presumably via solid-phase crystallization. By increasing the (average) laser power, elongated grain growth was visible which is typical for LPC of silicon.[3] A further increase of (average) laser power led to the dewetting of the silicon layer. Similarly, laser scan speed was optimized to achieve crack-free crystallization. To lower the thermal-induced stress during cooling, laser scan speed was lowered to decrease the thermal gradient between the layers of mismatching thermal expansion coefficients.[54] As a result and as shown in **Figure 11**, we were able to achieve (using our stable [porous] a-Si:H material) crack-free crystallized polycrystalline silicon with grain widths of several μm (see Figure 11b) and grain lengths of several mm. These values, however, are smaller than those reported by Haschke et al.[3] Figure 11a shows the top-view microscope image of crystallized silicon using an optimized (average) laser power of 50 W and a scan speed of 3 mm s^{-1}.

Our unstable (dense) a-Si:H material with laser-ablated lines (with distances <400 nm) was also subjected to laser LPC treatment. Such films did not peel and remained intact after the high temperature laser scan. However, the dense a-Si material suffers from bubble formation near the glass/ONO and amorphous silicon interface and also, the laser grooves remain visible after the LPC process. Therefore, molten a-Si material during LPC could not fill the groove spaces.

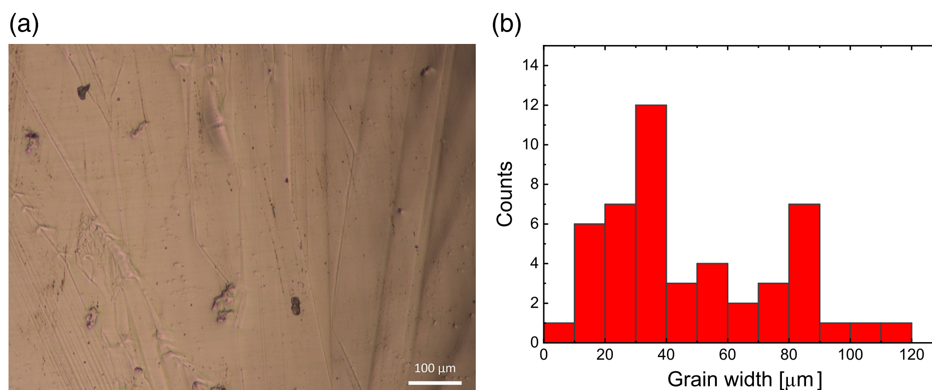

Figure 11. a) Microscope image of our liquid-phase crystallized silicon and b) grain width distribution histogram.

© 2021 The Authors. physica status solidi (a) applications and materials science published by Wiley-VCH GmbH

4. Discussion

The major result of this work is the finding that under suitable deposition conditions H can diffuse out of thick a-Si:H films rather rapidly so that after only 30 min heating up to 550 °C the films can be crystallized by the LPC process. Thus, an extended annealing procedure of at least 12 h at 550 °C to prevent peeling and disintegration for plasma-grown a-Si:H precursor layers appears unnecessary. Using the large-area thin-film silicon equipment, the production cost of this type of solar cell could thus decrease. Concerning the deposition conditions of the required (porous/reduced density) a-Si:H films, we note that those conditions involving various deposition parameters can likely be further optimized. While our results suggest that the enhanced diffusion of H is caused by the rapid motion of H_2 molecules, the details of this diffusion process have to be further clarified, in particular its dependence on the material microstructure. Furthermore, we note that columnar growth which apparently leads to porous a-Si:H has often been observed upon dilution of the precursor gases by Ar,[13,31] while the dilution of precursor gases with He, Ne, and Ar can increase the deposition rate.[55] Thus, provided that any incorporation of such gas atoms does not affect the LPC process, dilution by inert gases may lead to economic solutions with regard to deposition rate. The usefulness of H effusion measurements for such optimization is demonstrated in this work.

5. Conclusions

Our results show that by the choice of PECVD a-Si:H deposition conditions, a material can be grown that survives rapid heating to 550 °C (and H effusion) without peeling or bubble formation, due to a porous structure. This material can successfully be used as precursor for liquid phase crystallized silicon. Thus, for the development of economic thin-film crystalline silicon solar cells on glass, the deposition of precursor layers by PECVD may also be of interest. Material grown with a considerably higher deposition rate in a denser structure turned out to be rather unstable upon rapid heating. Peeling processes of thick films of dense a-Si:H were clarified.

Acknowledgements

The authors thank Dr. Elmar Neumann for SEM images, Gunnar Schöpe for help with the nanosecond laser system, and Helmholtz-Zentrum Berlin (HZB) LPC group for providing ONO interfacial layers. Support by Dirk Erdweg for the control of the hydrogen effusion apparatus is kindly acknowledged. The project was supported by the European Regional Development fund and the State Government of North Rhine-Westphalia in the framework of the Up-LLPC project (grant nos. EFRE-0800-561 and EU-1-2-037B).

Open access funding enabled and organized by Projekt DEAL.

Conflict of Interest

The authors declare no conflict of interest.

Keywords

amorphous silicon, annealing, liquid-phase crystallization, thermal stability

Received: July 8, 2020
Revised: October 30, 2020
Published online: March 31, 2021

[1] G. Andrä, J. Bergmann, F. Falk, *Thin Solid Films* **2005**, *487*, 77.
[2] G. Andrä, F. Falk, *Phys. Status Solidi C* **2008**, *5*, 3221.
[3] J. Haschke, D. Amkreutz, B. Rech, *Jpn. J. Appl. Phys.* **2016**, *55*, 04EA04.
[4] J. Haschke, D. Amkreutz, L. Korte, F. Ruske, B. Rech, *Sol. Energy Mater. Sol. Cells* **2014**, *128*, 190.
[5] M. A. Green, P. A. Basore, N. Chang, D. Clugston, R. Egan, R. Evans, D. Hogg, S. Jarnason, M. Keevers, P. Lasswell, J. O'Sullivan, U. Schubert, A. Turner, S. R. Wenham, T. Young, *Sol. Energy* **2004**, *77*, 857.
[6] S. Varlamov, B. Eggleston, J. Dore, R. Evans, D. Ong, O. Kunz, J. Huang, U. Schubert, K. H. Kim, R. Egan, M. Green, *Proc. SPIE* **2013**, *8608*, 86080Q.
[7] T. Sontheimer, C. Becker, F. Ruske, C. Klimm, U. Bloeck, S. Gall, O. Kunz, T. Young, R. Egan, J. Hüpkes, B. Rech, in *Proc. 35th IEEE Photovoltaic Specialists Conf.*, IEEE Electron Devices Society, Piscataway, NJ **2010**, pp. 614–619.
[8] D. Amkreutz, N. Preissler, C. Thi Trinh, M. Trahms, P. Sonntag, R. Schlatmann, B. Rech, *Prog. Photovoltaics Res. Appl.* **2018**, *26*, 524.
[9] O. Gabriel, T. Frijnts, S. Calnan, S. Ring, S. Kirner, A. Opitz, I. Rothert, H. Rhein, M. Zelt, K. Bhatti, J. H. Zollondz, A. Heidelberg, J. Haschke, D. Amkreutz, S. Gall, F. Friedrich, B. Stannowski, B. Rech, R. Schlatmann, *IEEE J. Photovoltaics* **2014**, *4*, 1343.
[10] Z. Said-Bacar, P. Prathap, C. Cayron, F. Mermet, Y. Leroy, F. Antoni, A. Slaoui, E. Fogarassy, *Appl. Surf. Sci.* **2012**, *258*, 9359.
[11] S. Garud, C. Thi Trinh, D. Abou-Ras, B. Stannowski, R. Schlatmann, B. Rech, D. Amkreutz, *Sol. RRL.* **2020**, *4*, 2000058.
[12] N. Preissler, D. Amkreutz, P. Sonntag, M. Trahms, R. Schlatmann, B. Rech, *Sol. RRL.* **2017**, *1*, 1700015.
[13] W. Beyer, *Sol. Energy Mater. Sol. Cells* **2003**, *78*, 235.
[14] A. Hofmann, S. Kambor, C. Schmidt, D. Grambole, J. Rentsch, S. W. Glunz, R. Preu, *Adv. OptoElectron.* **2008**, *2008*, 485467.
[15] J. Dore, R. Evans, B. D. Eggleston, S. Varlamov, M. A. Green, *Proc. MRS Symp.* **2012**, *1426*, 63.
[16] W. Beyer, H. Mell, in *Disordered Semiconductors* (Eds: M. A. Kastner, G. A. Thomas, S. R. Ovshinsky), Institute for Amorphous Studies Series, Springer, Boston, MA **1987**, pp. 641–659.
[17] C. Maurer, S. Haas, W. Beyer, F. C. Maier, U. Zastrow, M. Hülsbeck, U. Breuer, U. Rau, *Thin Solid Films* **2018**, *653*, 223.
[18] A. P. Sokolov, A. P. Shebanin, O. A. Golikova, M. M. Mezdrogina, *J. Non-Cryst. Solids* **1991**, *137–138*, 99.
[19] W. Beyer, F. Einsele, in *Advanced Characterization Techniques for Thin Film Solar Cells*, Wiley-VCH Verlag GmbH & Co. KGaA, Weinheim, Germany **2016**, pp. 569–595.
[20] O. Garcia, J. J. Garcia-Ballesteros, D. Munoz-Martin, S. Nunez-Sanchez, M. Morales, J. Carabe, J. Torres, J. J. Gandia, C. Molpeceres, *Appl. Surf. Sci.* **2013**, *278*, 214.
[21] C. Das, S. Ray, *J. Phys. D. Appl. Phys.* **2002**, *35*, 319.
[22] K. Ohdaira, T. Nishikawa, H. Matsumura, *J. Cryst. Growth* **2010**, *312*, 2834.
[23] N. A. Blum, C. Feldman, *J. Non-Cryst. Solids* **1972**, *11*, 242.
[24] W. Beyer, H. Wagner, *J. Non-Cryst. Solids* **1983**, *59–60*, 161.
[25] W. Beyer, in *Semiconductors and Semimetals* (Ed: N. H. Nickel), Vol. *61*, Academic Press, San Diego, CA **1999**, pp. 165–239.

© 2021 The Authors. physica status solidi (a) applications and materials science published by Wiley-VCH GmbH

[26] W. Beyer, *Phys. Status Solidi A* **2016**, *213*, 1661.
[27] D. E. Carlson, C. W. Magee, *Appl. Phys. Lett.* **1978**, *33*, 81.
[28] W. Beyer, H. Wagner, *J. Appl. Phys.* **1982**, *53*, 8745.
[29] W. Beyer, H. Wagner, *Le J. Phys. Colloq.* **1981**, *42*, C4-783.
[30] W. Beyer, in *Tetrahedrally-Bonded Amorphous Semiconductors* (Eds: D. Adler, H. Fritzsche), Institute for Amorphous Studies Series, Springer, Boston, MA **1985**, pp. 129–146.
[31] D. K. Biegelsen, R. A. Street, C. C. Tsai, J. C. Knights, *Phys. Rev. B.* **1979**, *20*, 4839.
[32] R. A. Street, C. C. Tsai, *Philos. Mag. B* **1988**, *57*, 663.
[33] C. Cushman, J. Zakel, L. S. Fisher, J. Banerjee, B. M. Lunt, N. S. Smith, M. R. Linford, *Vac. Technol. Coat.* **2018**, *23*.
[34] W. E. Spear, P. G. Le Comber, S. Kalbitzer, G. Müller, *Philos. Mag. B* **1979**, *39*, 159.
[35] J. Herion, W. Beyer, H. Wagner, *Surf. Interface Anal.* **1989**, *14*, 839.
[36] W. Beyer, *Proc. MRS Symp.* **2001**, *664*, A9.2.
[37] Y. Katayama, T. Shimada, K. Usami, E. Maruyama, *Le J. Phys. Colloq.* **1981**, *42*, C4-787.
[38] D. Beeman, R. Tsu, M. F. Thorpe, *Phys. Rev. B* **1985**, *32*, 874.
[39] O. A. Golikova, V. K. Kudoyarova, *Semiconductors* **1998**, *32*, 779.
[40] P. M. Voyles, N. Zotov, S. M. Nakhmanson, D. A. Drabold, J. M. Gibson, M. M. J. Treacy, P. Keblinski, *J. Appl. Phys.* **2001**, *90*, 4437.
[41] M. Ito, M. Kondo, *Jpn. J. Appl. Physics, Part 2 Lett.* **2006**, *45*, L230.
[42] F. Köhler, *PhD Thesis*, RWTH Aachen **2012**.
[43] P. Danesh, B. Pantchev, K. Antonova, F. Liarokapis, B. Schmidt, D. Grambole, J. Baran, *J. Phys. D Appl. Phys.* **2004**, *37*, 249.
[44] M. Cardona, *Phys. Status Solidi.* **1983**, *118*, 463.
[45] H. Wagner, W. Beyer, *Solid State Commun.* **1983**, *48*, 585.
[46] H. Shanks, C. J. Fang, L. Ley, M. Cardona, F. J. Demond, S. Kalbitzer, *Phys. Status Solidi* **1980**, *100*, 43.
[47] H. R. Shanks, L. Ley, *J. Appl. Phys.* **1981**, *52*, 811.
[48] C. Roch, J. C. Delgado, *Thin Solid Films* **1992**, *221*, 17.
[49] M. Serényi, C. Frigeri, Z. Szekrényes, K. Kamarás, L. Nasi, A. Csik, N. Q. Khánh, *Nanoscale Res. Lett.* **2013**, *8*, 1.
[50] S. Jafari, J. Steffens, M. Wendt, B. Terheiden, S. Meyer, D. Lausch, *Phys. Status Solidi B* **2020**, *257*, 2000097.
[51] S. Choi, O. Kwon, K. H. Min, M. S. Jeong, K. T. Jeong, M. G. Kang, S. Park, K. K. Hong, H. Song, K. H. Kim, *Sci. Rep.* **2020**, *10*, 9672.
[52] W. Beyer, W. Hilgers, D. Lennartz, F. C. Maier, N. H. Nickel, F. Pennartz, P. Prunici, *Proc. MRS Symp.* **2014**, *1666*, A14.
[53] B. Aspar, M. Bruel, H. Moriceau, C. Maleville, T. Poumeyrol, A. M. Papon, A. Claverie, G. Benassayag, A. J. Auberton-Hervé, T. Barge, *Microelectron. Eng.* **1997**, *36*, 233.
[54] T. Pliewischkies, T. Schmidt, I. Höger, J. Bergmann, A. Gawlik, G. Andrä, F. Falk, *Phys. Status Solidi A* **2015**, *212*, 317.
[55] J. C. Knights, R. A. Lujan, M. R. Rosenblum, R. A. Street, D. K. Biegelsen, J. A. Reimer, *Appl. Phys. Lett.* **1981**, *38*, 331.

© 2021 The Authors. physica status solidi (a) applications and materials science published by Wiley-VCH GmbH